

# Mössbauer parameters of $^{57}\text{Fe}$ substituents in the topological insulator $\text{Bi}_2\text{Se}_3$

Jorge H. Rodriguez\*

Department of Physics and Astronomy, Purdue University, West Lafayette, IN 47907, USA

$^{57}\text{Fe}$  Mössbauer spectroscopy can probe several *local* structural, electronic and magnetic properties of Fe-containing systems. However, to establish a direct relationship between these properties and a system's geometric structure, the experimental Mössbauer parameters need to be analyzed *via* electronic structure calculations. Herein, structural, electronic and magnetic effects of iron substituents in the topological insulator  $\text{Bi}_2\text{Se}_3$ , as uniquely probed by  $^{57}\text{Fe}$  Mössbauer spectroscopy, have been determined *via* spin-polarized electronic structure calculations. The iron ion substituents, of *nominal*  $\text{Fe}^{3+}$  ( $S = 5/2$ ) oxidation and spin state, are unequivocally shown to substitute  $\text{Bi}^{3+}$  sites in epitaxial  $\text{Bi}_2\text{Se}_3$  thin-films used for Mössbauer measurements. Concomitant with iron substitution, *localized* structural rearrangements take place whereby the longer Bi-Se bonds of the native system are replaced by significantly shorter Fe-Se counterparts in the Fe-containing system. The resulting distorted-octahedral environment about substituent iron ions gives rise to characteristic Mössbauer parameters ( $\delta_{\text{Fe}} \approx 0.51$  mm/s,  $\Delta E_{\text{Q}} \approx 0.20$  mm/s) which have been calculated in excellent agreement with measured values for Fe-doped  $\text{Bi}_2\text{Se}_3$  thin films. Consistent with a substituent  $\text{Fe}^{3+}$  ion's *nominal* high-spin electronic configuration ( $t_{2g}^{\uparrow\uparrow\uparrow}e_g^{\uparrow\uparrow}$ ), an Fe-centered spin density has been established which, nevertheless, extends towards neighboring Se atoms *via* direct Fe-Se bonding and concomitant Fe(d)-Se(p) hybridization.

## I. INTRODUCTION

Dibismuth triselenide ( $\text{Bi}_2\text{Se}_3$ ), a three-dimensional topological insulator (TI) and thermoelectric material, has a unit cell characteristically composed of three *quintuple* layers stacked along the  $c$  ( $z$ ) axis (Fig. 1). Intra-*quintuple* Bi-Se interactions are dominated by strong chemical bonding whereas inter-*quintuple* interactions are due to weaker van der Waal forces.<sup>1-3</sup> Whereas the Bi atoms of each *quintuple* are equivalent, there are two structurally-inequivalent Se layers whose atoms are herein denoted as Se(A) and Se(B). Some transition metal (TM) ions such as  $\text{Fe}^{3+}$  can act as  $\text{Bi}^{3+}$  substituents and, in addition to their net positive charge, carry a number of spin-unpaired electrons.  $\text{Fe}^{3+}$  ions in their high-spin configuration nominally carry five unpaired 3d-shell electrons leading to a sizable spin ( $S_{\text{Fe}} = 5/2$ ) and correspondingly high magnetic moment ( $\vec{\mu}_{\text{Fe}} = -g_s\mu_B\vec{S}_{\text{Fe}}/\hbar$ ). Interaction of the atomic orbitals of a substituent iron ion with those of neighboring, chemically-bound, Se atoms leads to some degree of Fe(3d) electron delocalization. This effect changes the *net* charge and magnetic moment of Fe substituents, relative to their *nominal* values, to a degree dependent on the host material's *immediate* electronic and structural environments.

Two parameters characteristic of an iron ion's electronic configuration and chemical-structural environment are directly measured by  $^{57}\text{Fe}$  Mössbauer spectroscopy, namely isomer shifts ( $\delta_{\text{Fe}}$ ) and quadrupole splittings ( $\Delta E_{\text{Q}}$ ). Spin-polarized electronic structure (SPES) calculations have been used to accurately predict structure-dependent  $^{57}\text{Fe}$  Mössbauer parameters<sup>4,5</sup> while, at the same time, establishing correlations with other properties of iron ions such as their *net* charges, magnetic moments, and spin densities.<sup>6</sup> Thus, by means of spin-polarized calculations one can establish correlations between Mössbauer parameters and concomitant elec-

tronic, magnetic and structural reorganizations of the host  $\text{Bi}_2\text{Se}_3$  material caused by iron substituents.

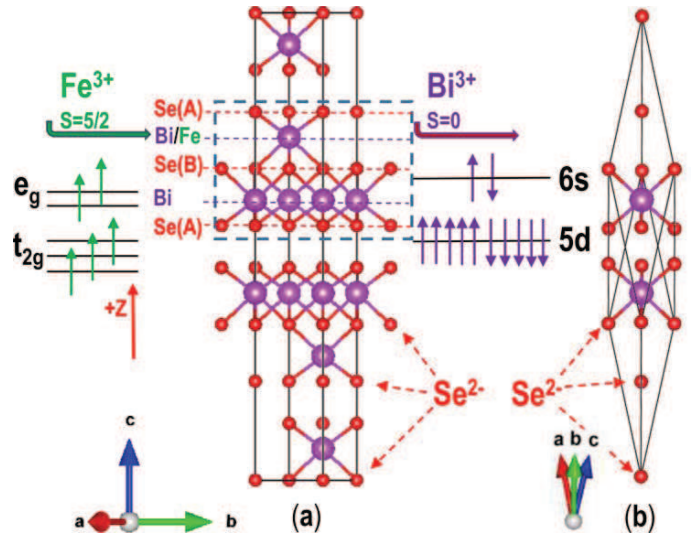


FIG. 1. (a) Unit cell of  $\text{Bi}_2\text{Se}_3$  displaying  $\text{Bi}^{3+}$  (purple) and  $\text{Se}^{2-}$  (red) ions. The three *quintuple* layers, stacked along the  $z$  axis, are displayed. The *local* environment of each Bi atom, in the presence of six chemically-bound Se atoms, is *distorted octahedral*. A magnetic  $\text{Fe}^{3+}$  ( $S=5/2$ ) ion substitutes a non-magnetic  $\text{Bi}^{3+}$  ( $S=0$ ) ion within a single *quintuple* layer which is enclosed in a dashed box. (b) Primitive cell displaying the Se-rich *distorted octahedral* environment of each Bi atom.

Although some experimental techniques probe magnetic properties of a bulk sample,  $^{57}\text{Fe}$  Mössbauer spectroscopy is a powerful technique to study *local* electronic, magnetic and structural properties of Fe substituents and their *immediate* structural environment. Fe-doped epitaxial  $\text{Bi}_2\text{Se}_3$  thin films and their conversion electron Mössbauer spectroscopy were reported by Pelenovich and coworkers<sup>7</sup> which provide raw values of the sample's iso-

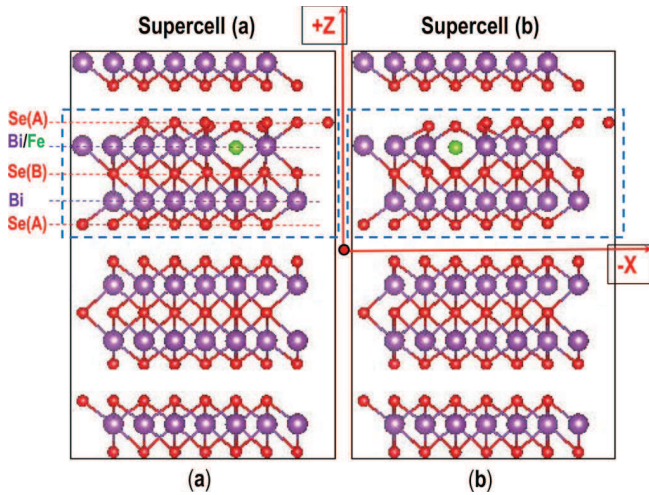


FIG. 2. Two structurally optimized  $3 \times 3 \times 1$   $\text{Bi}_2\text{Se}_3$  supercells, (a) and (b), each containing a magnetic iron substituent (green). Bi and Se atoms are shown in purple and red, respectively. The *quintuple* in each supercell containing the magnetic substituent is shown in a dashed box.

mer shift ( $\delta_{\text{Fe}}$ ) and quadrupole splitting ( $\Delta E_{\text{Q}}$ ). The latter parameters are generally highly dependent on the Fe-ion's immediate electronic-structural environment. More specifically,  $\delta_{\text{Fe}}$  and  $\Delta E_{\text{Q}}$  are sensitive to the structure-dependent 3d-shell electron configuration (e.g.  $t_{2g}^{\uparrow\uparrow\uparrow} e_g^{\uparrow\uparrow}$ ) and spherical or non-spherical symmetry of the combined electrostatic potential, at the site of the Fe nucleus, generated by valence electrons and/or surrounding crystalline lattice.

Doping with magnetic TM ions and/or their substitution for suitable counterparts in tetradymite topological insulators has been reported<sup>7-9</sup> and related samples studied by several techniques such as angle-resolved photoemission spectroscopy (ARPES), scanning tunneling microscopy (STM) and energy dispersive X-ray analysis (EDX).<sup>10-14</sup> Many studies have focused on the effects of TM doping on TI surface<sup>3,13,15</sup> and/or bulk states.<sup>10,16</sup> In particular, possible effects of the electric and magnetic properties of iron adatoms on topologically protected  $\text{Bi}_2\text{Se}_3$  surface states have been proposed.<sup>13,17-19</sup> However, the availability of conversion electron Mössbauer spectroscopy data<sup>7</sup> and its possible interpretation by means of *ab initio* SPES<sup>4</sup> allows the detailed investigation of other substitutional effects such as *local* Fe-centered structural changes in host  $\text{Bi}_2\text{Se}_3$  thin films and the emergence of partially delocalized spin densities about Fe substituents. The latter effects can be directly probed by SPES calculations and, indirectly, by  $^{57}\text{Fe}$  Mössbauer spectroscopy. Herein we use SPES to accurately predict  $^{57}\text{Fe}$  Mössbauer parameters and show that, upon  $\text{Fe}^{3+}$  for  $\text{Bi}^{3+}$  substitution, isomer shifts and quadrupole splittings of Fe-doped  $\text{Bi}_2\text{Se}_3$  thin films are directly dependent on the structural reorganization of neighboring Se atoms (Figs. 1-3) and, in addition, that an Fe-centered spin density emerges which propagates onto

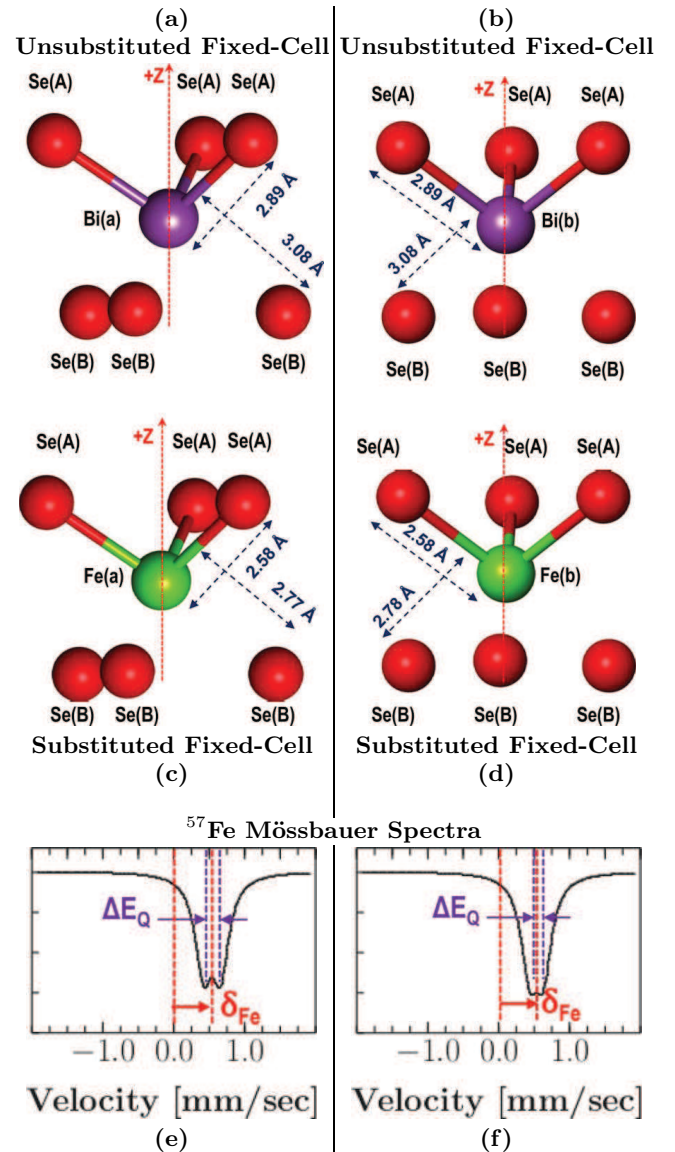


FIG. 3. (a,b) Se-rich local structural environments of Bi atoms in native  $\text{Bi}_2\text{Se}_3$  and (c,d) Fe atom substituents in  $\text{Bi}_2\text{Se}_3$ . Significantly different Bi-Se and Fe-Se bond lengths, corresponding to their respective optimized supercell structures, are shown. (e,f) Predicted absorption Mössbauer spectra for supercells (a) and (b), respectively, with  $\delta_{\text{Fe}}$  and  $\Delta E_{\text{Q}}$  values given in Table II and calculated for bond lengths and geometries given in (c)-(d). Predicted and experimental Mössbauer parameters are, within experimental accuracy, in agreement (Table II). Each predicted spectrum corresponds to two Lorentzian curves each of 0.28 mm/s width. For each spectrum the separation between the peaks of the two Lorentzians is the quadrupole splitting  $\Delta E_{\text{Q}}$ .

neighboring Se atoms (Figs. 4-5).

Upon Fe for Bi substitution ( $\text{Fe} \rightarrow \text{Bi}$ ) we have determined a significant Fe-centered structural reorganization of the native  $\text{Bi}_2\text{Se}_3$  host in qualitative agreement with previous studies.<sup>20,21</sup> A fairly *distorted octahedral* geometry about the Fe ions was found which is necessary to

reproduce measured Mössbauer parameters for Fe-doped thin films.<sup>7</sup> Strong Se-atom reorganization around the Fe substituents occurs whereby the former partially *collapse* onto the latter. Contrary to a nearly spherically symmetric spin distribution expected for  $\text{Fe}^{3+}$  ( $S=5/2$ ) in ionic environments, a cube-like Fe-centered spin density was found which nevertheless propagates onto neighboring Se atoms.

## II. THEORY AND METHODS

Spin-polarized gradient-corrected density functional theory was used to perform structural relaxations for both types of  $\text{Bi}_2\text{Se}_3$  structures, native and Fe-containing and, thereafter, generate electron densities needed to evaluate Mössbauer parameters. Two independent sets of calculations were performed on two different  $3 \times 3 \times 1$  supercells, labelled (a) and (b), whereby a different Bi site was substituted in each supercell by a corresponding Fe atom as shown in Fig. 2. Both substituted supercell structures were relaxed using identical SPES protocols giving rise to two, essentially equivalent, geometrically-distorted selenium-rich iron environments as shown in Figs. 3(c,d). This is consistent with all Bi atoms, such as Bi(a) and Bi(b), in the unsubstituted supercells being structurally equivalent to each other and, therefore, their respective geometrically-optimized iron substituents, Fe(a) and Fe(b), also being equivalent to each other. Each  $3 \times 3 \times 1$  supercell included 135 atoms.

For each supercell two types of structural relaxations were done: fixed-cell and variable-cell. The former kept lattice parameters frozen while optimizing intracell atomic positions whereas the latter relaxed both, lattice parameters and atomic positions. All structural optimizations used the Perdew-Burke-Ernzerhof exchange-correlation functional.<sup>22</sup> Fixed-cell optimizations used localized orbital basis of DZP quality<sup>23</sup> with norm-conserving relativistically-corrected pseudopotentials as reported by Rivero *et al.*<sup>24</sup> Variable-cell relaxations used the basis and relativistic effective core potentials of Stevens *et al.*<sup>25</sup>.

Mössbauer parameters are sensitive to structural variations. To compare calculated values of  $\delta_{\text{Fe}}$  and  $|\Delta E_{\text{Q}}|$  against experiment and to study their dependence on various geometric environments, four types of Fe-containing structures were used for each of the two supercells:

- I. Substituted Fixed-Cell
- II. Substituted Variable-Cell
- III. Unsubstituted Fixed-Cell [Bi $\rightarrow$ Fe]
- IV. Unsubstituted Variable-Cell [Bi $\rightarrow$ Fe]

Structures I and II correspond to the dimensions obtained for Fe-substituted supercells *via* fixed-cell [Figs. 3(c,d)] and variable-cell relaxations, respectively. Structures III and IV correspond to the dimensions obtained for unsubstituted supercells *via* fixed-cell

[Figs. S1(c,d)]<sup>26</sup> and variable-cell relaxations, respectively, with subsequent replacement of Fe for Bi atoms: [Bi(a) $\rightarrow$ Fe(a)] and [Bi(b) $\rightarrow$ Fe(b)]. Supp. Fig. S1<sup>26</sup> illustrates structures III-IV and Supp. Table S1<sup>26</sup> lists some metric parameters for all, I-IV, structures.

Prediction of Mössbauer parameters requires evaluation of electron densities at the site of the iron nucleus. Some authors have used *augmented* plane wave density functional methods to evaluate electron densities at the nucleus.<sup>27,28</sup> Herein, following pseudopotential-based supercell optimization, further all-electron calculations with Gaussian-type basis on Fe-centered clusters allowed evaluation of electron densities at the origin. By using a locally developed Mössbauer program<sup>4</sup> prediction of Mössbauer parameters was achieved. Knowledge of ground state electron densities,  $\rho_{\text{o}}(\mathbf{r})$ , in turn allows evaluation of ground state energies ( $E_{\text{o}}$ ) as functionals of the density:

$$\rho_{\text{o}}(\mathbf{r}) = \sum_i |\phi_i^{\uparrow}(\mathbf{r})|^2 + \sum_j |\phi_j^{\downarrow}(\mathbf{r})|^2 \quad (1)$$

$$E_{\text{o}} = E_{\text{o}}[\rho_{\text{o}}(\mathbf{r})] \quad (2)$$

Here, the sets  $\{\phi_i^{\uparrow}(\mathbf{r})\}$  and  $\{\phi_j^{\downarrow}(\mathbf{r})\}$  correspond to occupied Kohn-Sham orbitals hosting spin-up and spin-down electrons, respectively. A *formally*  $\text{Fe}^{3+}$  substituent has a majority of spin-up unpaired 3d-shell electrons which results in the number of spin-up and spin-down occupied Kohn-Sham orbitals being different. This fact, in turn, determines the overall system's net spin state and, for Fe-doped  $\text{Bi}_2\text{Se}_3$ , mainly reflects the presence of an Fe-centered magnetic moment. Thus, the system's spin density,  $\rho_{\text{s}}(\mathbf{r})$ , as defined in Eq. 3 is also expected to be Fe-centered in agreement with the numerical results presented in Fig. 4:

$$\rho_{\text{s}}(\mathbf{r}) = \sum_i |\phi_i^{\uparrow}(\mathbf{r})|^2 - \sum_j |\phi_j^{\downarrow}(\mathbf{r})|^2 \quad (3)$$

The physical origin of the Mössbauer parameters can be understood in terms of Eq. (4) for the isomer shift and Eq. (5) for the quadrupole splitting:

$$\delta_{\text{Fe}} = \frac{2\pi}{3} Z e^2 (\langle R^2 \rangle^* - \langle R^2 \rangle) \{ \rho_{\text{Ab}}(r=0) - \rho_{\text{So}}(r=0) \} \quad (4)$$

$$\Delta E_{\text{Q}} = \frac{1}{2} e Q V_{zz} (1 + \eta^2/3)^{\frac{1}{2}} \quad (5)$$

$$\eta \equiv (V_{xx} - V_{yy})/V_{zz} \quad (6)$$

In a Mössbauer experiment a moving  $^{57}\text{Co}$  radioactive source (So) emits a Doppler-shifted 14.4 KeV  $\gamma$ -ray that excites the nucleus of an absorbing (Ab) Fe ion. In Eq. (4) the difference  $-e\{\rho_{\text{So}}(r=0) - \rho_{\text{Ab}}(r=0)\}$ , corresponding to electron charge densities at the sites of the emitting source and absorbing nuclei, interacts with the nuclear charge  $Ze$ .<sup>4</sup> The term  $(\langle R^2 \rangle^* - \langle R^2 \rangle)$  is the difference of mean square charge radii corresponding to nuclear excited and ground states, respectively.<sup>29</sup> In a series of  $^{57}\text{Fe}$  Mössbauer experiments this nuclear radii difference and  $\rho_{\text{So}}(r=0)$  are regarded as constants and only the term  $\rho_{\text{Ab}}(r=0)$  varies for different samples.

The SPES calculations evaluate characteristic electron densities at the nuclei of substituent Fe ions,  $\rho_{\text{Ab=Fe}}(r=0)$ , in the Se-rich environment of the  $\text{Bi}_2\text{Se}_3$  host. Knowledge of electron densities at iron nuclei allowed computation of Mössbauer isomer shifts which, due to electron density - nuclear charge interactions, are sensitive to the Fe ion's electronic charge distribution, magnetic moment and immediate structural-chemical environment. Importantly, Mössbauer calculations were performed for geometric parameters corresponding to both, before and after, Fe-induced reorganization of  $\text{Bi}_2\text{Se}_3$ . Mössbauer parameters were significantly different for relaxed Fe-substituted and relaxed Fe-unsubstituted supercell structures. Predicted isomer shifts were compared with experimentally measured values for Fe-doped  $\text{Bi}_2\text{Se}_3$  thin films. Similarly, by evaluating the components of the electric field gradient (EFG) tensor at the Fe nuclei ( $V_{xx}$ ,  $V_{yy}$ ,  $V_{zz}$ ), which are sensitive to the asymmetric positions of  $\text{Se}^{2-}(\text{A})$  versus  $\text{Se}^{2-}(\text{B})$  ions, we calculated electric quadrupole splittings ( $\Delta E_Q$ ) which were also compared against experiment.

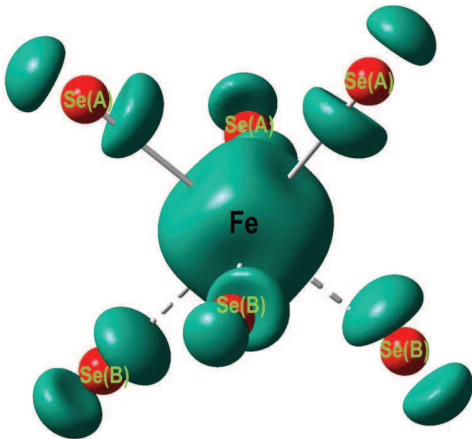


FIG. 4. Three-dimensional plot (in green) of the Fe-centered spin density,  $\rho_s(\mathbf{r})$ , partially delocalized towards the neighboring  $\text{Se}(\text{A})$  and  $\text{Se}(\text{B})$  atoms. The green region corresponds to a greater accumulation of majority (spin up), relative to minority (spin down), electrons.

### III. RESULTS AND DISCUSSION

Both computed parameters,  $\delta_{\text{Fe}}$  and  $\Delta E_Q$ , were in excellent agreement with experiment but only *after* Fe-induced geometric reorganization of the  $\text{Bi}_2\text{Se}_3$  host was taken into account. This corresponds to the “Substituted Fixed-Cell” optimizations illustrated by Figs. 3(c,d). Due to their slightly different geometric parameters “Substituted Variable-Cell” structures displayed close but slightly different Mössbauer values (Supp. Table S1<sup>26</sup>). By contrast, Mössbauer values associated with the longer Fe-Se bond lengths of all “Unsubstituted ( $\text{Bi} \rightarrow \text{Fe}$ )” structures were significantly different from ex-

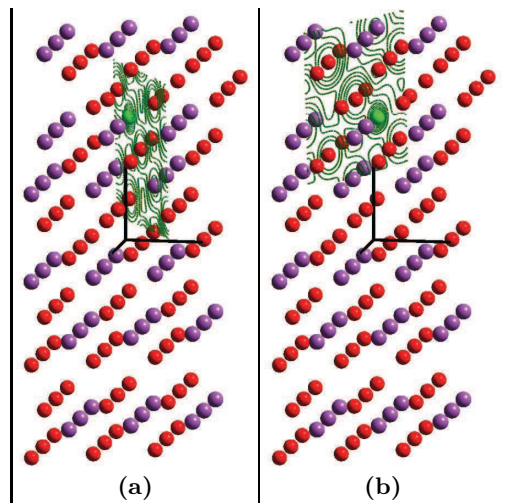


FIG. 5. Two-dimensional contour plots (in green) of the spin density in quasi-perpendicular planes defined by a)  $\text{Se}(\text{B})$ - $\text{Fe}(\text{A})$ - $\text{Se}(\text{A})$  and b)  $\text{Se}(\text{A})$ - $\text{Fe}(\text{A})$ - $\text{Se}(\text{B})$ . Isosurface value for contours set to 0.008.

periment. In summary, parameters obtained from all “Substituted” fixed-cell and variable-cell optimizations displayed similar trends and were in qualitative agreement with each other. Results obtained for all “Unsubstituted ( $\text{Bi} \rightarrow \text{Fe}$ )” structures were consistent within their own group. This indicates that it is the presence or absence of Fe-centered reorganization corresponding to the former or latter structures, respectively, that results in Mössbauer observables in agreement or disagreement with experiment. Table II shows results for “Substituted Fixed-Cell” relaxed structures and, for comparison, Supp. Table S1<sup>26</sup> includes all other results.

#### A. Structural Effects of Fe Substitution

Table I displays lattice parameters of the  $\text{Bi}_2\text{Se}_3$  unit cell<sup>1,2</sup> where the hexagonal structure of the undoped system imposes the condition  $a = b \neq c$ . Upon substitution of an Fe ion in lieu of a Bi ion, followed by structural optimization without any symmetry constraints, the overall hexagonal condition was essentially maintained. The relaxed (i.e. energy-minimized) Fe-containing  $3 \times 3 \times 1$  supercells displayed a nearly negligible difference between the parameters  $a$  and  $b$  which are perpendicular to the  $c$  axis. This minimal asymmetry may reflect the finite size, despite being fairly large, of the  $3 \times 3 \times 1$  supercells whose structures were optimized without symmetry constraints to ensure that substituent Fe ions occupy their most energetically-favorable locations. Despite the overall Fe-unsubstituted and Fe-substituted lattice parameters remaining nearly identical, consistent with EXD measurements<sup>14</sup>, *localized* intra-cell structural variations about the Fe ions were much more noticeable. As shown in Fig. 3(c,d), relaxed interatomic distances for the Fe-containing system [ $\text{Fe-Se}(\text{A})$ : 2.58Å,  $\text{Fe-Se}(\text{B})$ : 2.77Å]

were substantially shorter than corresponding lengths [Bi-Se(A): 2.89Å, Bi-Se(B): 3.08Å] of the relaxed, but unsubstituted, Bi<sub>2</sub>Se<sub>3</sub> structure.

The present results are qualitatively consistent with previous structural relaxation studies that found neighboring Se atoms moving towards the TM ions, with more distant atoms displaying much smaller structural variations,<sup>20</sup> and significant displacement towards chromium or iron atoms resulting in shorter Se-Cr or Se-Fe bond lengths, respectively.<sup>21</sup>

TABLE I. Structural parameters of native (unsubstituted) and Fe-containing (substituted) Bi<sub>2</sub>Se<sub>3</sub> unit cells.

	Lattice Constants					
	a [Å]	b [Å]	c [Å]	$\alpha$ [deg]	$\beta$ [deg]	$\gamma$ [deg]
Native (Exp.) <sup>1</sup>	4.143	4.143	28.636	90.000	90.000	120.000
Native (Exp.) <sup>2</sup>	4.138	4.138	28.64	90.000	90.000	120.000
Native <sup>a</sup>	4.234	4.239	28.731	90.002	89.998	119.961
Fe(A)-Substituted <sup>a</sup>	4.225	4.229	28.758	89.997	89.999	119.966
Fe(B)-Substituted <sup>a</sup>	4.225	4.229	28.757	89.998	90.002	119.997

<sup>a</sup> Variable-cell computational relaxation

## B. Mössbauer Parameters of <sup>57</sup>Fe Substituents

Considering their *local* structural environment, Fe<sup>3+</sup> ions which substitute Bi<sup>3+</sup> counterparts, are in a *distorted octahedral* environment. As illustrated by Fig. 1(a) such crystalline distortion gives rise to energy splittings between the iron ion's 3d-electron sub-shells, namely  $t_{2g}^X$  and  $e_g^Y$  where X and Y represent the electron occupations

TABLE II. Bond lengths, atomic magnetic moments ( $|\vec{\mu}|$ )<sup>a</sup> and calculated <sup>57</sup>Fe Mössbauer isomer shifts ( $\delta_{Fe}$ ) and electric quadrupole splittings ( $\Delta E_Q$ ) for optimized geometries of two Fe-containing Bi<sub>2</sub>Se<sub>3</sub> supercells.<sup>b</sup> Experimental<sup>7</sup> Mössbauer parameters for Fe-doped Bi<sub>2</sub>Se<sub>3</sub> also shown.

Supercell	Site	Fe-Se(A)	Fe-Se(B)	$ \vec{\mu} $	$\delta_{Fe}$	$ \Delta E_Q $
		[Å]	[Å]	[ $\mu_B$ ]	[mm/s]	[mm/s]
(a)	Fe(a)	2.582	2.773	3.677	(+)0.514	0.209
	Se(A)			0.126		
	Se(B)			0.051		
(b)	Fe(b)	2.580	2.775	3.681	(+)0.497	0.184
	Se(A)			0.128		
	Se(B)			0.051		
Average (a), (b)					(+)0.506	0.197
Exp. <sup>7</sup>					(+)0.44	0.23
					$\pm 0.1$	$\pm 0.07$

<sup>a</sup> Magnetic moments in units of Bohr magneton.

<sup>b</sup> Fe-Se distances correspond to fixed-cell optimizations (Table I)

of each sub-shell. To elucidate the origin of spectroscopic parameters one can use the *formal* number,  $N = X + Y$ , of 3d-shell electrons which for the more common oxidation states Fe<sup>2+</sup> and Fe<sup>3+</sup> is  $N = 6$  and  $N = 5$ , respectively. The <sup>57</sup>Fe Mössbauer parameters of the substituent atoms were consistent with *nominal*  $t_{2g}^3 - e_g^2$  electronic configurations. However, non-negligible effects of 3d-shell electron delocalization were also present as manifested in the magnitudes of magnetic moments ( $|\vec{\mu}|$ ) for iron ions and their selenium-bound neighbors. Table II shows that a *nominal*  $|\vec{\mu}| = 5 \mu_B$  moment corresponding to ionic Fe<sup>3+</sup> ( $S = 5/2$ ) reduces, in a Bi<sub>2</sub>Se<sub>3</sub> environment, to  $\approx 3.68 \mu_B$  while the *nominally* diamagnetic Se<sup>2-</sup> ions acquire small moments of  $\approx 0.13$  and  $\approx 0.05 \mu_B$  for Se(A) and Se(B), respectively. These results are consistent with the Fe-centered, but Se-delocalized, spin densities shown in Figs. 4-5.

Whereas, depending on the local crystalline fields, Fe<sup>3+</sup> ions can be in high ( $S = 5/2$ ), intermediate ( $S = 3/2$ ) or low ( $S = 1/2$ ) spin states, their computed electronic configurations and hyperfine interactions, as substituents in the Bi<sub>2</sub>Se<sub>3</sub> host, were consistent with *nominal* Fe<sup>3+</sup> ( $S = 5/2$ ) states. This is reflected in the predicted <sup>57</sup>Fe Mössbauer parameters ( $\delta_{Fe} \approx 0.51$  mm/s,  $\Delta E_Q \approx 0.20$  mm/s, Table II) which are, within experimental accuracy, in excellent agreement with experiment for structurally relaxed Fe-containing Bi<sub>2</sub>Se<sub>3</sub> supercells.

Both parameters, isomer shifts and quadrupole splittings, are fairly sensitive to the distorted octahedral environments of the iron ions. The latter parameter, in particular, reflects the inequivalence of Fe-Se(A) and Fe-Se(B) bond lengths. This geometric asymmetry produces minor electric field gradients (EFG) at the iron nuclei and in turn, *via* Eq. 5, fairly small electric quadrupole splittings ( $|\Delta E_Q|$ ). Predicted ( $\approx 0.20$  mm/s) and experimental (0.23 mm/s) values were, within the reported experimental uncertainty ( $\pm 0.07$  mm/s)<sup>7</sup>, in agreement.

For other electronic configurations of iron, such as Fe<sup>2+</sup> ( $S = 4/2$ ), a more sizable electric field gradient generated by 3d-shell electrons can yield substantially larger electric quadrupole splittings. Thus, in the present case, the presence of Fe<sup>2+</sup> electronic configurations can be ruled out for being inconsistent with the measured Mössbauer parameters. By contrast, for Fe<sup>3+</sup> ( $S = 5/2$ ) ions in distorted octahedral environments, the 3d-shell contributes little to the EFG and its main contribution arises from the crystal lattice. The EFG at the nuclei of Fe<sup>3+</sup> substituents in Bi<sub>2</sub>Se<sub>3</sub> thin films used for Mössbauer measurements, and consequently their  $\Delta E_Q$  values, mainly originates in the asymmetric position of an iron atom relative to Se<sup>2-</sup> (A) *versus* Se<sup>2-</sup> (B) ions.

Our findings that iron substituents in the reported Mössbauer sample are in a *nominal* Fe<sup>3+</sup> state are consistent with EXD observations<sup>14</sup> that sample annealing suppresses the presence of Fe<sup>2+</sup> and facilitates substitution of Fe<sup>3+</sup> for Bi<sup>3+</sup>. Likewise, the Mössbauer parameters are inconsistent with other possible locations of the substituents, such as interstitial sites within *inter-quintuple*

van der Waal regions, as different values for  $\delta_{\text{Fe}}$  and/or  $\Delta E_{\text{Q}}$  would be expected. Indeed previous studies suggest that Fe for Bi substitution is more energetically favorable than interstitial doping.<sup>30,31</sup>

### C. Spectroscopic and Structural Correlations

Being a *local* probe Mössbauer spectroscopy measures parameters which are sensitive to the structural, chemical and electronic properties of an Fe ion's *immediate* environment. One expects shorter or longer Fe-Se bond lengths, within a  $\text{Bi}_2\text{Se}_3$  host lattice, to be reflected in the measured values of  $\delta_{\text{Fe}}$  and  $\Delta E_{\text{Q}}$ . The significantly different Fe-Se bond lengths corresponding to “Substituted Fixed Cell” *versus* “Unsubstituted Fixed Cell (Bi $\rightarrow$ Fe)” structures, summarized in Table S1<sup>26</sup>, are expected to yield correspondingly different Mössbauer parameters. Although the Fe substituents in a particular Mössbauer sample may correspond to a specific geometric environment, computationally it is possible to study  $\delta_{\text{Fe}}$  and  $\Delta E_{\text{Q}}$  as a function of geometry. Accordingly, we computed structure-dependent Mössbauer parameters for two different Fe ion environments corresponding to the dimensions of energy-minimized i) “Substituted Fixed Cell” and ii) “Unsubstituted Fixed Cell (Bi $\rightarrow$ Fe)” structures. We recall that the first type has shorter Fe-Se bond lengths in comparison to the second type which has longer bonds. Since both typed of structures were obtained by means of the same SPES protocol it is possible to directly compare their bond lengths and other metric parameters. As expected, computed Mössbauer parameters for both types of structures were substantially different and only those corresponding to the first type, with reorganized iron environments as shown in Figs. 3(c,d), were in agreement with experiment (Table II). For comparison Mössbauer results for these and other structures are listed in Supp. Table S1<sup>26</sup>.

The different  $\delta_{\text{Fe}}$  and  $\Delta E_{\text{Q}}$  values calculated for different iron environments, show that Mössbauer spectroscopy is sensitive to structural variations. The discrepancy between experimental Mössbauer values with those corresponding to “Unsubstituted Fixed Cell (Bi $\rightarrow$ Fe)” geometries, in contrast with the excellent agreement obtained for those with reorganized Fe environments (“Substituted Fixed Cell”), confirms that the structural and bonding environments of  $\text{Fe}^{3+}$  ions in the particular sample used for Mössbauer measurements<sup>7</sup> are very closely

described by Figs. 3(c,d).

## IV. SUMMARY

Mössbauer spectroscopy probes the *local* electronic, magnetic and structural environments of  $^{57}\text{Fe}$  substituents in crystalline environments. Conversion electron Mössbauer measurements were performed on Fe-doped epitaxial thin films by Pelenovich *et al.*<sup>7</sup> However, to establish a direct correlation between measured Mössbauer parameters and the geometric structure of Fe-substituted  $\text{Bi}_2\text{Se}_3$ , *ab initio* quantum mechanical analysis was needed. Accordingly, the present SPES calculations explain the relationship between geometric structure and Mössbauer properties of substituted  $\text{Bi}_2\text{Se}_3$  in the limit of low iron concentration. In this limit, predicted structure-dependent Mössbauer parameters were in excellent agreement with experiment.

As  $\text{Fe}^{3+}$  substitutes  $\text{Bi}^{3+}$  we found a substantial, yet *localized*, structural reorganization which yields Fe-Se distances significantly shorter than corresponding Bi-Se bonds in the undoped structure. It is within this restructured environment that substituted iron yields the experimentally observed Mössbauer parameters. We have shown that  $\text{Fe}^{3+}$  ions in a very specific system, namely the reported epitaxial thin-film Mössbauer sample,<sup>7</sup> are in a *local* distorted-octahedral Se-rich environment. Although experimental Mössbauer parameters have been reported for epitaxial  $\text{Bi}_2\text{Se}_3$  films, essentially the same behavior is expected for low concentration of Fe doping in single crystals if and when  $\text{Fe}^{3+}$  explicitly substitutes  $\text{Bi}^{3+}$ . Correlations between geometric, electronic and magnetic properties for Fe-substituted  $\text{Bi}_2\text{Se}_3$  have been established. An Fe-centered spin density is reported which extends towards neighboring chemically-bound Se atoms *via* direct Fe-Se bonding and concomitant hybridization of Fe(d) and Se(p) orbitals. The substituted structure, therefore, has magnetic moments mainly centered on iron ( $\approx 3.68 \mu_{\text{B}}$ ) with small, but finite, contributions from its neighboring Se(A) ( $\approx 0.13 \mu_{\text{B}}$ ) and Se(B) ( $\approx 0.05 \mu_{\text{B}}$ ) atoms.

**Acknowledgement.** Access to high performance computing facilities by Purdue University’s ITaP center is gratefully acknowledged.

\* jhrodrig@purdue.edu

<sup>1</sup> S. Nakajima, Journal of Physics and Chemistry of Solids **24**, 479 (1963).  
<sup>2</sup> R. Wyckoff, *Crystal Structures - Volume 2: Inorganic Compounds R<sub>2</sub>Xn, RnMX<sub>2</sub>, RnMX<sub>3</sub>* (Interscience Publishers, 1964).  
<sup>3</sup> J. P. Heremans, R. J. Cava, and N. Samarth, Nature Reviews Materials **2**, 17049 EP (2017), review Article.  
<sup>4</sup> J. H. Rodriguez, Hyperfine Interactions **217**, 73 (2013).  
<sup>5</sup> T. Chachiyo and J. H. Rodriguez, Dalton Trans. **41**, 995 (2012).  
<sup>6</sup> R.-N. Wang, J. H. Rodriguez, and W.-M. Liu, Phys. Rev. B **89**, 235414 (2014).  
<sup>7</sup> V. O. Pelenovich, R. Xiao, Y. Liu, P. Liu, M. Li, Y. He,

- and D. Fu, *Thin Solid Films* **577**, 119 (2015).
- <sup>8</sup> V. A. Kulbachinskii, A. Y. Kaminsky, K. Kindo, Y. Narumi, K. ichi Suga, P. Lostak, and P. Svanda, *Physica B: Condensed Matter* **329-333**, 1251 (2003).
  - <sup>9</sup> J. S. Dyck, P. Hájek, P. Lošťák, and C. Uher, *Phys. Rev. B* **65**, 115212 (2002).
  - <sup>10</sup> F. Yang, Y. R. Song, H. Li, K. F. Zhang, X. Yao, C. Liu, D. Qian, C. L. Gao, and J.-F. Jia, *Phys. Rev. Lett.* **111**, 176802 (2013).
  - <sup>11</sup> D. Hsieh, D. Qian, L. Wray, Y. Xia, Y. S. Hor, R. J. Cava, and M. Z. Hasan, *Nature* **452**, 970 EP (2008).
  - <sup>12</sup> S.-Y. Xu, M. Neupane, C. Liu, D. Zhang, A. Richardella, L. Wray, N. Alidoust, M. Leandersson, T. Balasubramanian, J. Sanchez-Barriga, O. Rader, G. Landolt, B. Slomski, H. Dil, J. Osterwalder, T.-R. Chang, H.-T. Jeng, H. Lin, A. Bansil, and M. Z. Hasan, *Nature Physics* **8**, 616 (2012).
  - <sup>13</sup> Y. L. Chen, J.-H. Chu, J. G. Analytis, Z. K. Liu, K. Igarashi, H.-H. Kuo, X. L. Qi, S. K. Mo, R. G. Moore, D. H. Lu, M. Hashimoto, T. Sasagawa, S. C. Zhang, I. R. Fisher, Z. Hussain, and Z. X. Shen, *Science* **329**, 659 (2010).
  - <sup>14</sup> L. Lv, D. Zhou, M. Zhang, L. Yang, X. Yang, and Y. Zhao, *Materials Letters* **99**, 118 (2013).
  - <sup>15</sup> Q. Liu, C.-X. Liu, C. Xu, X.-L. Qi, and S.-C. Zhang, *Phys. Rev. Lett.* **102**, 156603 (2009).
  - <sup>16</sup> G. Rosenberg and M. Franz, *Phys. Rev. B* **85**, 195119 (2012).
  - <sup>17</sup> L. A. Wray, S.-Y. Xu, Y. Xia, D. Hsieh, A. V. Fedorov, Y. S. Hor, R. J. Cava, A. Bansil, H. Lin, and M. Z. Hasan, *Nature Physics* **7**, 32 EP (2010).
  - <sup>18</sup> J. Honolka, A. A. Khajetoorians, V. Sessi, T. O. Wehling, S. Stepanow, J.-L. Mi, B. B. Iversen, T. Schlenk, J. Wiebe, N. B. Brookes, A. I. Lichtenstein, P. Hofmann, K. Kern, and R. Wiesendanger, *Phys. Rev. Lett.* **108**, 256811 (2012).
  - <sup>19</sup> M. R. Scholz, J. Sánchez-Barriga, D. Marchenko, A. Varykhalov, A. Volykhov, L. V. Yashina, and O. Rader, *Phys. Rev. Lett.* **108**, 256810 (2012).
  - <sup>20</sup> P. Larson and W. R. L. Lambrecht, *Phys. Rev. B* **78**, 195207 (2008).
  - <sup>21</sup> J.-M. Zhang, W. Ming, Z. Huang, G.-B. Liu, X. Kou, Y. Fan, K. L. Wang, and Y. Yao, *Phys. Rev. B* **88**, 235131 (2013).
  - <sup>22</sup> J. P. Perdew, K. Burke, and M. Ernzerhof, *Phys. Rev. Lett.* **77**, 3865 (1996).
  - <sup>23</sup> J. M. Soler, E. Artacho, J. D. Gale, A. García, J. Junquera, P. Ordejón, and D. Sánchez-Portal, *Journal of Physics: Condensed Matter* **14**, 2745 (2002).
  - <sup>24</sup> P. Rivero, V. M. Garca-Surez, D. Pereiguez, K. Utt, Y. Yang, L. Bellaiche, K. Park, J. Ferrer, and S. Barraza-Lopez, *Computational Materials Science* **98**, 372 (2015).
  - <sup>25</sup> W. J. Stevens, M. Krauss, H. Basch, and P. G. Jasien, *Canadian Journal of Chemistry* **70**, 612 (1992).
  - <sup>26</sup> See Supplemental Material at [ ] for i) additional figures describing the unsubstituted fixed-cell structures and ii) a table summarizing computed Mössbauer parameters for all structures described in the text.
  - <sup>27</sup> J. W. Zwanziger, *Journal of Physics: Condensed Matter* **21**, 195501 (2009).
  - <sup>28</sup> P. Blaha, *Journal of Physics: Conference Series* **217**, 012009 (2010).
  - <sup>29</sup> G. K. Wertheim, in *Applications of the Mössbauer Effect in Chemistry and Solid State Physics*, Technical Reports Series No. 50 (IAEA, Vienna, 1966).
  - <sup>30</sup> X. Wei, J. Zhang, B. Zhao, Y. Zhu, and Z. Yang, *Physics Letters A* **379**, 417 (2015).
  - <sup>31</sup> J.-M. Zhang, W. Zhu, Y. Zhang, D. Xiao, and Y. Yao, *Phys. Rev. Lett.* **109**, 266405 (2012).